Simulation and optimization of dopant-free asymmetric heterojunction solar cells*

ZHENG Qiaoqiao[1], YUAN Yujie[1], HOU Guofu[2], LI Wei[1], TAO Ke[1], and PENG Zhuo[1]**

1. Tianjin Key Laboratory of Film Electronic and Communication Devices, School of Integrated Circuit Science and Engineering, Tianjin University of Technology, Tianjin 300384, China

2. Institute of Photoelectronic Thin Film Devices and Technology, Nankai University, Tianjin 300350, China

(Received 28 September 2022; Revised 19 November 2022)

In order to further study doping-free asymmetric heterojunction (DASH) solar cells, we used AFORS-HET software to optimize the structure of Al/SnO_2/a-Si:H (i)/c-Si (p)/a-Si:H (i)/NiO_x/Ag. In a certain adjustment range, a series of simulations were carried out on the band gap, electron affinity, thickness and work function (*WF*) of NiO_x, thickness and *WF* of SnO_2, and the thickness of a-Si:H (i). After the above optimization, 21.08% efficiency was obtained at 300 K. This study shows that the solar cells with this structure have good light absorption properties in a very wide spectrum. The present simulation provides instructive suggestions for follow-up experiments of DASH solar cells.

Document code: A **Article ID:** 1673-1905(2023)06-0337-10

DOI https://doi.org/10.1007/s11801-023-2159-1

Currently, the development of crystalline silicon cells has led to two important technical solutions: changing the absorption rate of incident light, and improving the selective contact of carriers. Both solutions improve the performance of solar cells. Interdigitated back contact (IBC) solar cells are configured to improve the absorption rate of incident light. Although the current efficiency of IBCs has reached 26.7%, the fabrication process is complex and requires multiple lithography to determine the dimensions of the hole transport layer (HTL) and electron transport layer (ETL). Therefore, IBCs are not conducive to large-scale production. Moreover, the manufacture processes require a high temperature that causes problems such as carrier recombination. To improve the selective contact of carriers, researchers have developed various kinds of silicon-based solar cells, such as silicon heterojunction (SHJ) and tunnel oxide passivated contact (TOPCon) solar cells. However, the HTLs and ETLs in these cells are realized by doping of amorphous silicon (or polycrystalline silicon layers), which brings multiple problems. First, doping easily forms defect trap centers, resulting in serious recombination of carriers. Second, the amount of dopant must be precisely controlled. If the doping is too small, the carrier transport is inhibited because amorphous silicon is poor in conducting. Conversely, excessive doping causes severe carrier recombination and a high defect density. Third, the narrow band gap of amorphous silicon is prone to serious parasitic absorption[1]. For these reasons, replacements of amorphous silicon doped HTL/ETL are now being sought.

Dopant-free asymmetric heterojunction (DASH) solar cells appeared. In 2014, BATTAGLIA et al[2] directly deposited a 15-nm-thick MoO_x layer on crystalline silicon (c-Si (n)) as a hole-selective contact using the thermal evaporation method, and an efficiency of 14.3% was obtained. In 2016, BULLOCK et al[1] passivated the front and rear surfaces of silicon substrate by depositing intrinsic hydrogenated amorphous silicon (a-Si:H (i)) on both sides of silicon substrate. Then, the hole-selective contact was MoO_x and the electron-selective contact was LiF_x. The open circuit voltage and efficiency were V_{oc}=714 mV and η=19.4%, respectively. In 2018, BULLOCK et al[3] inserted a layer of TiO_x between amorphous silicon and LiF_x to realize a device with 20.7% efficiency. They found that TiO_x played not only a passivation role, but also a stabilizing role. In 2019, ZHONG et al[4] grew MoO_x by thermal evaporation and reported a large band gap and an improved work function (*WF*). Covering ZnO films with LiF/Al can improve the electron selectivity and suppress parasitic infrared absorption, boosting the efficiency to 21.4%[4]. This efficiency is the highest yet reported for undoped asymmetric solar cells.

DASH solar cells retain the advantages of HIT cells while improving the shortcomings of HIT amorphous silicon doping[3,4]. The intrinsic amorphous silicon passivation layer in DASH solar cells prevents both carrier recombination and the energy band mismatch between the metal oxide and the monocrystalline silicon substrate

* This work has been supported by the National Natural Science Foundation of China (Nos.62074084 and No.62074165).

** E-mail: yjyuan@email.tjut.edu.cn

on which it resides. The amorphous silicon doped HTL/ETL is replaced with oxides, fluorides and other materials with low *WFs*. The different *WFs* of the contacting materials ensure the extraction and transport of carriers and prevent the serious recombination of carriers, poor conductivity, and complex process caused by doping. A structure with both high and low *WFs* also has a relatively wide band gap that reduces parasitic light absorption.

MoO_x, WO_3, V_2O_5, and NiO_x are materials with high *WFs*, whereas TiO_x, ZnO, and SnO_2 have low *WFs*. Nickel oxide is a p-type direct band gap semiconductor[5] with a wide band gap, high *WF*, low electron affinity, and high hole mobility[6]. It is further advantaged by high optical transmittance, sufficient electrical conductivity, high chemical stability, an effective electron blocking layer, and low cost. Accordingly, NiO_x has been widely used in novel optoelectronic devices and p-n heterojunctions. NiO_x has an energy band gap in the range of E_g=3.6—4.3 eV[7], an electron affinity in the range of χ=1.1—1.7 eV[8], and a *WF* in the range of *WF*=5.0—5.6 eV[9]. All of these parameters are adjustable. NiO_x films exist in mixed forms with Ni $(OH)_2$, NiOOH, Ni_2O_3 (Ni^{3+} species)[10], NiO, Ni, and $(NiSi_x)$[11]. NiO_x itself exists in three phases, namely Ni, Ni^{2+}, and Ni^{3+}[12]. Purely stoichiometric NiO is a typical Mott-Hubbard insulator but exhibits charge transfer properties[7]. SUN et al[13] proposed an oxygen-enriched preparation method for films with interstitial oxygen, which generates Ni^{2+} vacancies and facilitates the formation of Ni^{3+} ions. The presence of Ni^{3+} ions increases the p-type conductivity of NiO_x films. Meanwhile, the conductivity of NiO_x can be adjusted by optimizing the surface modification or processing method[7]. Most of the existing perovskite solar cells are based on NiO_x and their performance exceeds 20%. Therefore, we introduce a NiO_x thin film as the HTL of our solar cell structure.

When selecting the ETL material, we considered the four requirements of the ETL in an optoelectronic device, including high charge transfer and hole blocking ability, high electron mobility, high transmittance to reduce optical loss, and high chemical stability[14,15]. Tin oxide offers the additional advantages of excellent optical properties, high electrical conductivity, deep conduction and valence bands, and a wide band gap. To date, the highest efficiency of perovskite solar cells with a SnO_2 ETL is 25.2%[16]. Therefore, our configuration includes SnO_2 as the ETL. The electron affinity of undoped SnO_2 is 4 eV. The direct band gap of SnO_2 is 3.59 eV, but here we use the experimentally measured band gap of SnO_2, namely, 3.6 eV[17]. The *WF* varies from 3.9 eV to 4.46 eV[16] depending on the processing method and surface modification technique. Therefore, we selected SnO_2 as the ETL in our solar cell structure.

At present, the mechanism of DASH solar cells remains unclear. Proposed models have shown only a close relationship between the cell mechanism and the performance of the cell materials. To clarify this situation, we simulated a DASH solar cell using AFORS-HET software. The efficiency of the DASH solar cell was optimized by adjusting the electron affinity, band gap, thickness, *WFs* of the HTL and ETL, intrinsic amorphous silicon thickness, device test temperature, and other parameters. Our work provided effective approaches for optimizing DASH solar cell structures and improving the cell performance.

Fig.1 shows the structure and energy band diagram of the DASH solar cell simulated using AFORS-HET software. The model is based on one-dimensional Poisson equation and continuity equation. The structure of the simulated solar cell is Al/SnO_2/a-Si:H (i)/c-Si (p)/a-Si:H (i)/NiO_x/Ag and the corresponding parameters are listed in Tabs.1 and 2. The surface recombination velocities of the holes and electrons were both set to 1.0×10^7 cm/s. AM1.5 solar spectrum light source was used, the operating temperature was set to 300 K, and the reflectivity of the front and rear surface was set to 0.1 and 1, respectively.

In this simulation, we investigated the effect of the NiO_x energy band gap E_g (3.6—4.3 eV) on the performance of the DASH solar cells. (a)—(d) of Fig.2 plotted the open-circuit voltage (V_{oc}), short-circuit current density (J_{SC}), fill factor (*FF*) and conversion efficiency η of the solar cell as a function of E_g.

When the E_g of NiO_x increased from 3.6 eV to 3.9 eV, V_{oc} remained unchanged because no splitting of holes and electrons occurred at the quasi-Fermi energy (quasi-E_f) level throughout the device in this band gap region. The *FF* and η increased from 45.6% to 53.65% and from 12.26% to 14.71%, respectively. The η change was mainly elicited by *FF*, which itself might be affected by charge injection and with the increase of the band gap width, the Fermi energy level decreased, holes were injected into the adjacent a-Si-H (i) layer, which increased the hole concentration in the adjacent a-Si-H (i) layer and reduced the resistivity. Increasing E_g of NiO_x from 3.9 eV to 4.3 eV caused only a slight change in V_{oc}. Meanwhile, J_{sc} decreased from 39.51 mA/cm^2 to 5.916 mA/cm^2, *FF* decreased from 53.65% to 6.248%, and η decreased from 14.71% to 0.2568%, because the barrier of hole transport to NiO_x increased. Therefore, the optimal band gap of NiO_x in this solar cell was 3.9 eV, the optimal V_{oc} was 693.8 mV, J_{sc} was 39.51 mA/cm^2, *FF* was 53.65%, and η was 14.71%. Our simulation results were consistent with the previously observed insulator-like behavior of NiO_x with a band gap of 4.3 eV[7].

The electron affinity of NiO_x was tunable from 1.1 eV to 1.7 eV and exerts a certain influence on the device performance. The simulation results were shown in Fig.3. As χ increased from 1.1 eV to 1.4 eV, V_{oc} decreased and partially recovered at χ=1.3 eV, remaining constant thereafter. Meanwhile, J_{sc} increased from 38.02 mA/cm^2 to 39.51 mA/cm^2, *FF* increased from 40.58% to 53.66%, and η increased from 10.72% to

14.71%. It was presumed that when χ increased from 1.1 eV to 1.4 eV, the barrier height decreased and the migration of minority carriers increased and the reason for the increase of *FF* was that with the increase of NiO_x affinity, the Fermi energy level decreases, and holes were injected into the adjacent a-Si-H (i) layer, so that the hole concentration of the adjacent a-Si-H (i) layer increased and the resistivity decreased.

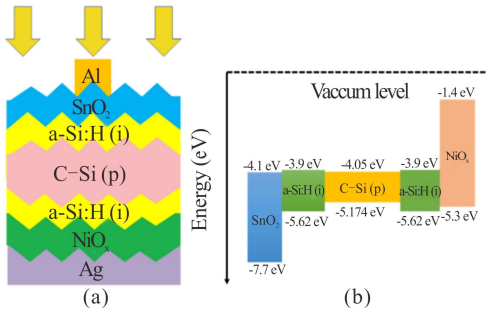

Fig.1 (a) Structure and (b) energy band diagram of the undoped asymmetric heterojunction solar cell investigated in this study

Tab.1 Parameters of the simulated DASH solar cells[18-20]

Parameter	SnO_2	a-Si-H (i)	c-Si (p)	NiO_x
Layer thickness (nm)	Variable	Variable	2.5×10^5	Variable
Dielectric constant (d_k)	9	11.9	11.9	10
Electron affinity (χ, eV)	4	3.9	4.05	1.1—1.7
Band gap (E_g, eV)	3.6	1.72	1.124	3.6—4.3
Effective conduction band density (N_c, cm^{-3})	2.2×10^{17}	1×10^{20}	2.8×10^{19}	2.8×10^{19}
Effective valence band density (N_v, cm^{-3})	2.2×10^{16}	1×10^{20}	2.6×10^{19}	1×10^{19}
Effective electron mobility (μ_n, $cm^2V^{-1}s^{-1}$)	20	20	1 041	12
Effective hole mobility (μ_p, $cm^2V^{-1}s^{-1}$)	10	5	412.9	2.8
Doping concentration of acceptors (N_a, cm^{-3})	0	0	5×10^{17}	1×10^{18}
Doping concentration of donors (N_d, cm^{-3})	1×10^{18}	0	0	0
Thermal velocity of electrons (V_e, $cm\cdot s^{-1}$)	1×10^7	1×10^7	1×10^7	1×10^7
Thermal velocity of holes (V_h, $cm\cdot s^{-1}$)	1×10^7	1×10^7	1×10^7	1×10^7
Layer density (ρ, $g\cdot cm^{-3}$)	2.328	2.328	2.328	2.328

When χ was further increased from 1.4 eV to 1.7 eV, all parameters decreased except V_{oc}, which remained unchanged. η decreased from 14.71% to 9.356%, J_{sc} decreased from 39.51 mA/cm^2 to 37.71 mA/cm^2, and *FF* decreased from 53.66% to 35.76%. At χ values exceeding 1.4 eV, the energy band could easily form a high potential barrier that blocks hole migration from c-Si (p) to NiO_x. Therefore, we selected χ=1.4 eV as the best electron affinity of NiO_x in the cell.

Tab.2 Simulation parameter settings of the front and rear electrodes[21]

Electrode parameter	Front electrode	Black electrode
Material	Al	Ag
Thickness	200 nm	200 nm
Optical properties	n=1.19; k=7.05	Ag with default n and k

Fig.4 plotted the performance parameters as the NiO_x thickness increased from 1 nm to 9 nm. The band gap of NiO_x was set to 3.9 eV and the electron affinity energy was set to 1.4 eV, and other conditions remained unchanged. Increasing the NiO_x thickness notably decreased the J_{sc}, *FF*, and η from 40.56 mA/cm^2 to 39.57 mA/cm^2, from 57.43% to 53.51%, and from 16.16% to 14.69%, respectively, but did not affect the V_{oc}. It was inferred that increasing the film thickness increased the series resistance, thus worsening the conductivity, hindering the transport of holes, and eventually reducing the *FF* and efficiency. The thickness independence of V_{oc} could be explained by the unchanged *WF* at the interfaces. In an ultra-thin NiO_x film, the *WF* and hole concentration will markedly increase and the device performance will improve. A thin and conductive NiO_x film rather than thick intrinsic insulators was needed because of its high bonding energy. In such a cell, the device performance responded to nanometer-scale thickness differences. However, the film deposited on a randomly pyramid shaped device should be at least 1.5 nm because a thinner film could not fully cover the surface[3]. In the structure simulated in this study, the a-Si:H (i) could easily contact the metal, resulting in carrier recombination. To meet the performance requirement of the experiment, the thickness of 1.5 nm was chosen as the optimal value for NiO_x films.

We varied the *WF* of NiO_x from 5.0 eV to 5.6 eV[9] and investigated its effect on the device performance. As shown in Fig.5, the V_{oc}, J_{sc}, *FF*, and η initially increased with increasing *WF* and eventually flattened. Increasing the *WF* of NiO_x increased the *WF* difference between NiO_x and the interface (Fig.6), thus enhancing the bending of the induced energy band and improving the efficiency. The *WF* difference could generate a strong built-in electric field that improved the separation ability of the photo-generated carriers. The extraction of hole was enhanced. The eventual flattening of the *WF* at 5.4—5.6 eV could be explained by bending and matching of the high potential barrier generated in NiO_x and

its interface, which hinders the electron backflow. As the *WF* of NiO_x could not exceed 5.5 eV at present[22], we selected 5.5 eV as the *WF* of NiO_x in subsequent simulations. Under this condition, we

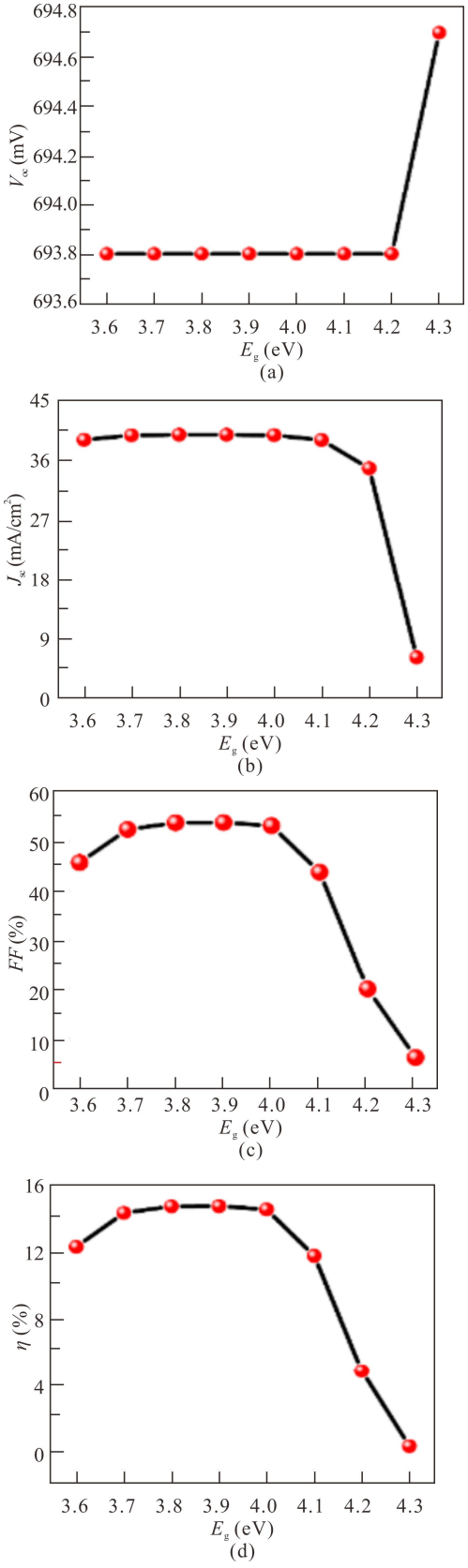

Fig.2 Performance parameters of DASH solar cells versus NiO_x band gap: (a) V_{oc}; (b) J_{sc}; (c) *FF*; (d) η

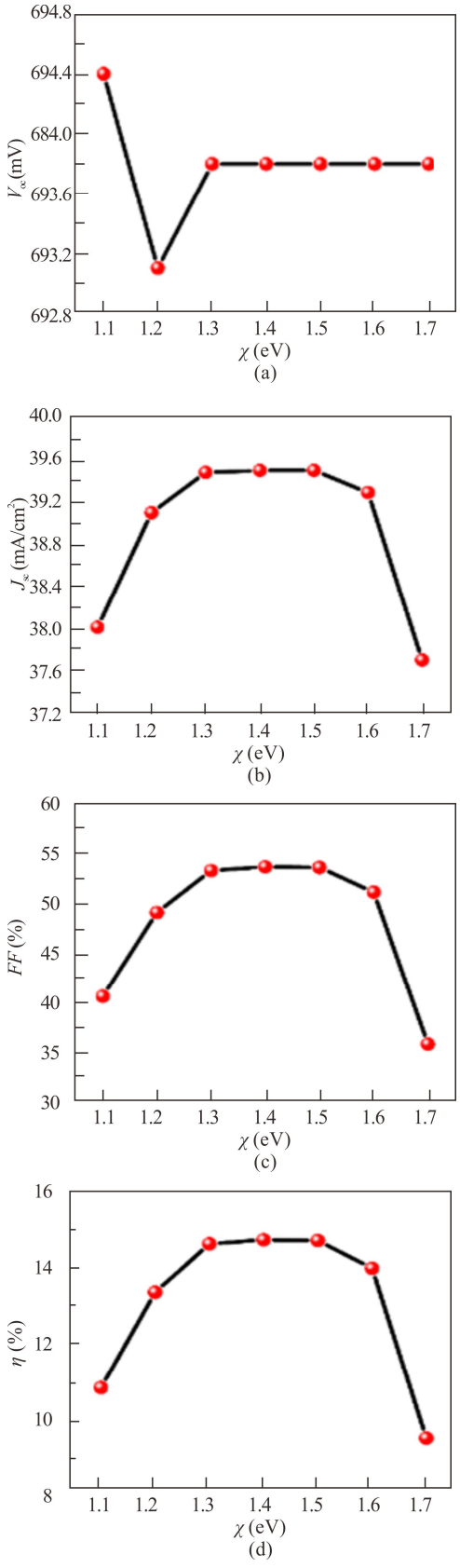

Fig.3 Performance parameters versus NiO_x electron affinity in DASH solar cells: (a) V_{oc}; (b) J_{sc}; (c) *FF*; (d) η

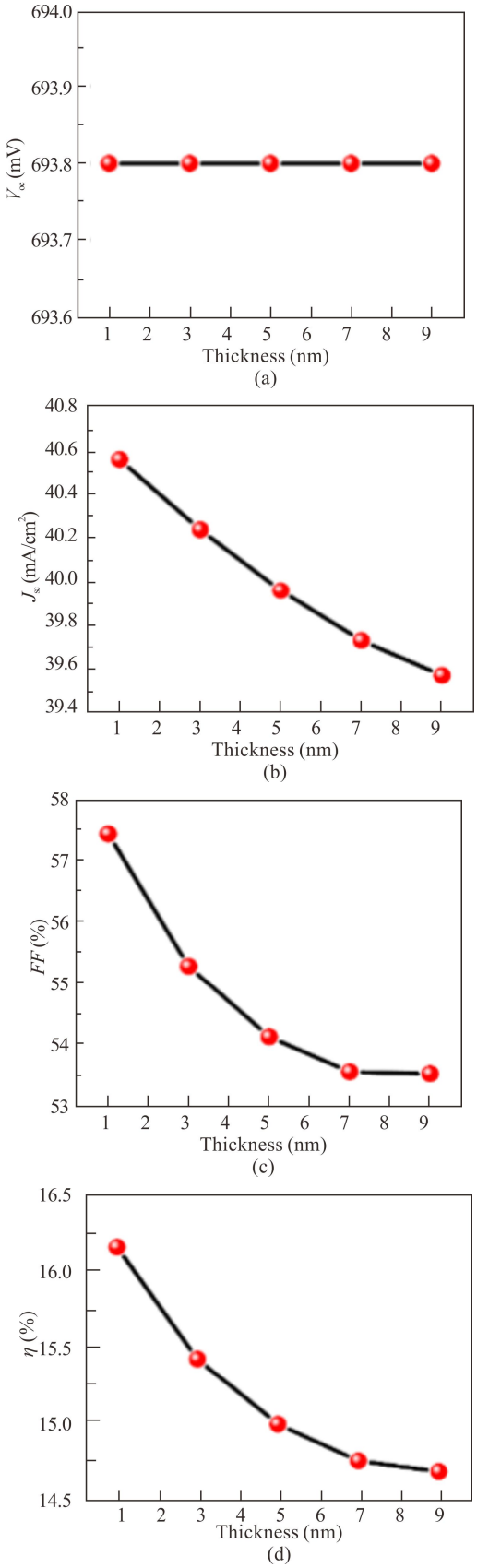

Fig.4 Performance parameters versus NiO_x thickness in DASH solar cells: (a) V_{oc}; (b) J_{sc}; (c) *FF*; (d) η

obtained V_{oc}=697 mV, J_{sc}=41.24 mA/cm^2, *FF*=62.28%, and η=17.91%.

SnO_2 constitutes the window and electron transport layer in solar cells and its thickness greatly influence the device performance. As shown in Fig.7, increasing the thickness of the SnO_2 layer gradually decreased the device performance. An internal structure analysis revealed several advantages of a very thin, dense ETL: fast extraction of electrons, a short diffusion length that suppresses carrier recombination, and high transmittance of the window layer, which enhanced the number of photo-generated carriers and hence improved the device performance. In the DASH solar cell, a 1-nm-thick SnO_2 layer yielded the highest efficiency (26.67%) and the V_{oc} of 723.4 mV, the J_{sc} of 43.8 mA/cm^2, and the *FF* of 18%. When the SnO_2 thickness increased to 10 nm, the V_{oc}, J_{sc}, and *FF* decreased to 697 mV, 41.24 mA/cm^2, and 62.28%, respectively, and η was 17.91%. The V_{oc} is mainly affected by the reverse saturation current density, which was mainly determined by junction recombination and surface recombination. The carrier recombination was affected by the interface properties and energy band differences. Here, the change in V_{oc} could be explained by the lengthened diffusion length of SnO_2, which increased the recombination rate of carriers and thereby reduced the device performance. The J_{sc} depended on the number of photo-generated carriers. A thicker window layer reduced the light transmission and hence the number of photo-generated carriers, so the J_{sc} decreased. A thin dense layer increased the J_{sc} by reducing the series resistance. However, if the SnO_2 layer was too thin, pinholes were easily generated in the experimental preparation. As pinholes leak charged[14], they increased the likelihood of carrier recombination. To minimize the pinholes and series resistance, the thickness of SnO_2 film should be around 2 nm[15]. We therefore set the SnO_2 thickness to 2 nm in the simulation study.

Selecting the appropriate *WF* value was very important for the ETL, because the PN junction of dopant-free asymmetric heterojunction solar cells extracted photo-generated carriers through the asymmetric surface-band bending generated by the high and low *WFs* of the HTL and ETL. The surface energy and of the film with the lower *WF* bend downward, enabling smooth flow of the photo-generated electrons into the ETL. The wide band gap prevented carrier recombination by blocking the flow of photo-generated holes, which was called electron-selective contact. Conversely, the surface energy band of the film with a high *WF* bends upward, allowing the efficient transport of photo-generated holes while blocking photo-generated electrons. This opposite phenomenon is called hole-selective contact[11]. Therefore, the *WF* of the metal oxide in DASH solar cells must be tuned to optimize the energy level shift. Since the electron affinity of SnO_2 was set to 4.0 eV in the simulation, the calculated range of *WF* was from 4.1 eV to 4.5 eV.

As evidenced in Fig.8, the V_{oc}, J_{sc}, *FF*, and η decreased as the *WF* increased from 4.1 eV to 4.5 eV. The

V_{oc} decreased noticeably from 705.6 mV to 694.1 mV, the η reduced from 23.85% to 14.11% owing to losses in *FF* and V_{oc}. These phenomena could be understood from the energy band diagrams in Fig.9. As the *WF* of SnO_2 increased, the energy band mismatched between SnO_2 and its interface reduced, thus lessening the bending of the induced energy band and lowering the collection of photo-generated electrons. The V_{oc} was lowered accordingly. The bending amplitude of the energy band was maximized at 0.42 eV when the *WF* was 4.1 eV. The band bending amplitude decreased to 0.18 eV when the *WF* increased to 4.5 eV. Therefore, a suitable *WF* was essential for the collection of electrons and holes. Here, the *WF* of SnO_2 was selected as 4.1 eV.

As is well known, monocrystalline silicon substrates contain many defects near the surface. Therefore, the surface must be modified by a passivation layer that diminished the surface defects. The a-Si:H (i) layer passivates the dangling bonds on the surface of monocrystalline silicon, converting them to Si-H-Si bonds and realizing a long minority-carrier lifetime. Such a condition was important for maintaining high V_{oc}, high efficiency, and an excellent temperature coefficient. Insertion of an a-Si:H (i) layer was the typical passivation method used in SHJs, and other solar cells. Therefore, this excellent passivation structure has also been adopted in DASH solar cells[3,4].

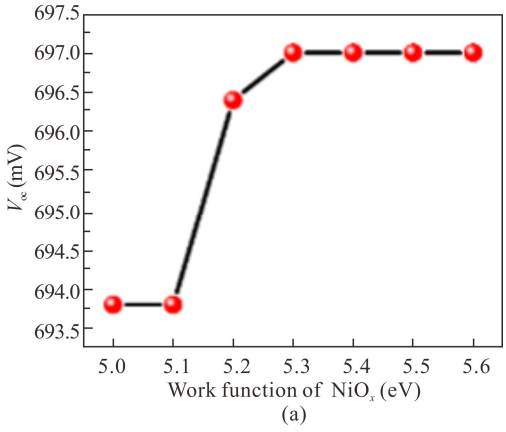

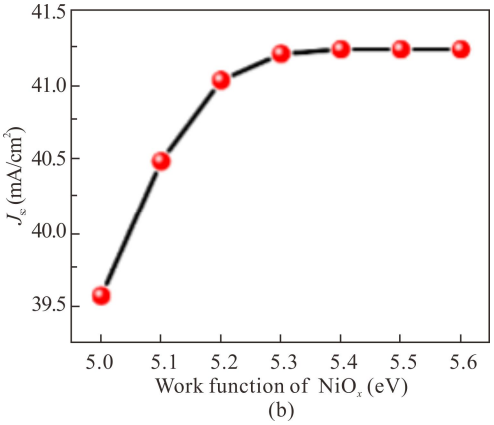

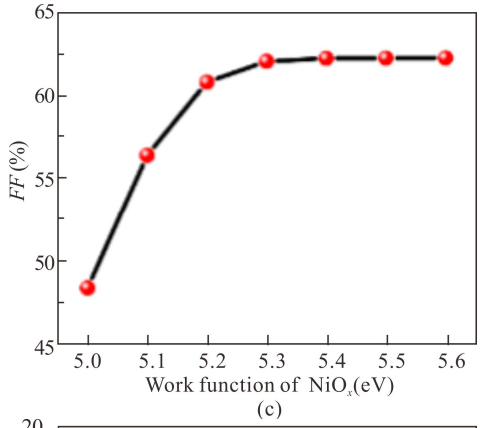

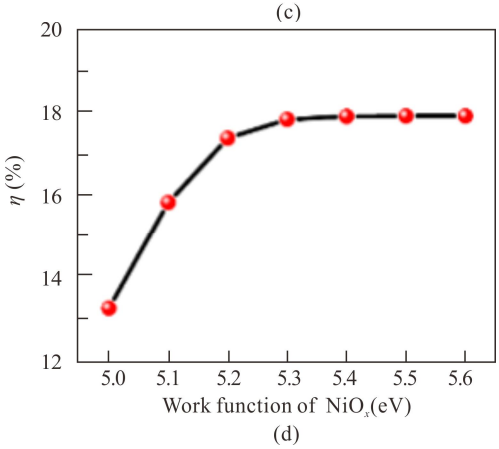

Fig.5 Performance parameters versus NiO_x *WF* in DASH solar cells: (a) V_{oc}; (b) J_{sc}; (c) *FF*; (d) η

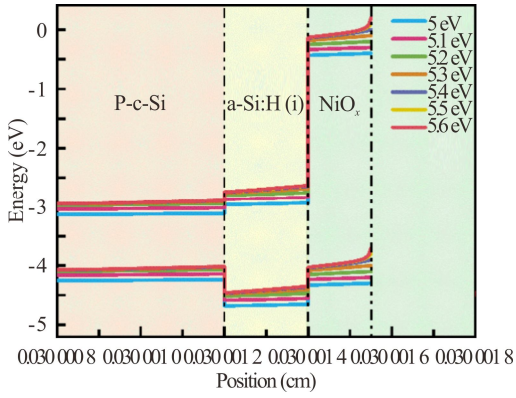

Fig.6 Energy band diagrams of NiO_x with different *WFs*

However, as the conductivity of intrinsic amorphous silicon was sub-excellent, the thickness of the a-Si:H (i) passivation layer must be properly adjusted. From the perspective of passivation performance, intrinsic amorphous silicon was grown by plasma enhanced chemical l vapor deposition (PECVD). The thicker the film, the better the passivation effect (V_{oc}). However, an excessively thick film will lead to optical parasitic absorption loss (J_{sc}) and electrical loss (*FF*). Therefore, in the actual preparation process, the thickness of intrinsic amorphous silicon film was controlled to be at least 3 nm. If it is too thin, the coating property of amorphous silicon on the surface pyramid will be poor and the passivation performance

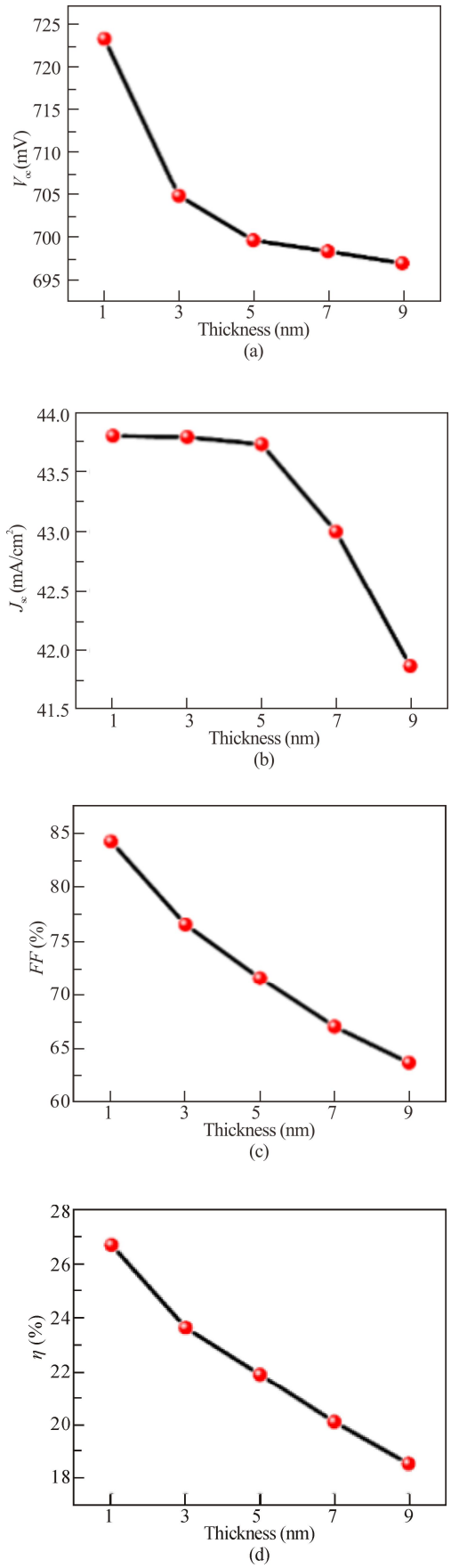

Fig.7 Performance parameters versus SnO_2 thickness in DASH solar cells: (a) V_{oc}; (b) J_{sc}; (c) *FF*; (d) η

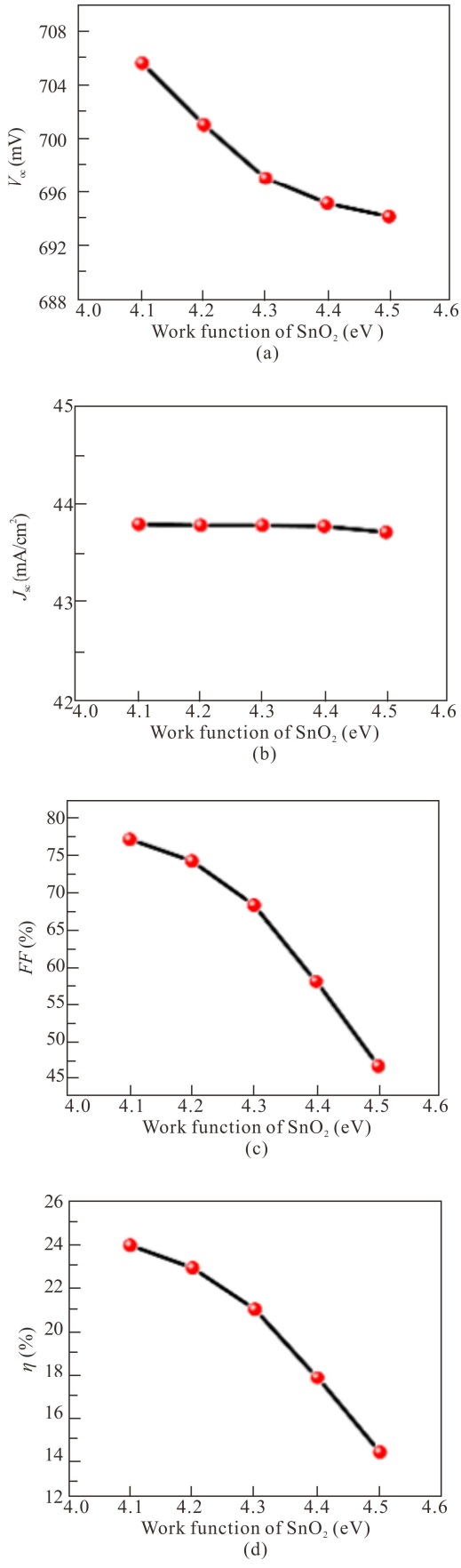

Fig.8 Performance parameters versus SnO_2 *WF* in DASH solar cells: (a) V_{oc}; (b) J_{sc}; (c) *FF*; (d) η

will be reduced. An excessively thin layer will incompletely cover the substrate, leaving contact points between SnO_2 and the monocrystalline silicon substrate. At these contact points, serious recombination of carriers occurs. Meanwhile, an excessively thick a-Si:H (i) passivation layer will increase the series resistance, resulting in loss of *FF* and efficiency. We thus varied the thicknesses of the front and rear passivation layers from 1 nm to 5 nm and observed their effects on the performance of DASH solar cells. The simulation results are plotted in Fig.10. The parameters were maximized when the front and rear passivation layers were both 1 nm in thick: η=27.03%, V_{oc}=724.7 mV, J_{sc}=44.22 mA/cm^2, and *FF*=84.33%. When the front and rear passivation layers were 5 nm in thick, η, V_{oc}, J_{sc}, and *FF* were reduced to 15.2%, 677.3 mV, 39.51 mA/cm^2, and 56.82%, respectively. The reduction of V_{oc} as the thickness increased from 1 nm to 5 nm could be explained by the longer diffusion distance in the thicker a-Si:H (i), which increased the likelihood of carrier recombination across the interfaces during the transport process. Meanwhile, the J_{sc} could be decreased by optical losses in the front passivation layer as the a-Si:H (i) thickness increased. These losses reduce the number of photo-generated carriers. Increasing the thicknesses of the front and rear passivation layers might also increase the series resistance. To identify the more important of these two possibilities, we carried out spectral simulations of the external quantum efficiency (*EQE*) and internal quantum efficiency (*IQE*) in systems with different a-Si:H (i) thicknesses. The spectra were not obviously changed by increasing the a-Si:H (i) thickness from 1 nm to 3 nm (Fig.11), indicat ing that the thickness-dependent efficiency change was driven by excessive series resistance. Thethickness-dependen t decrease of J_{sc} from 4 nm might reflect the simultaneous influences of both of the abovementioned possibilities.

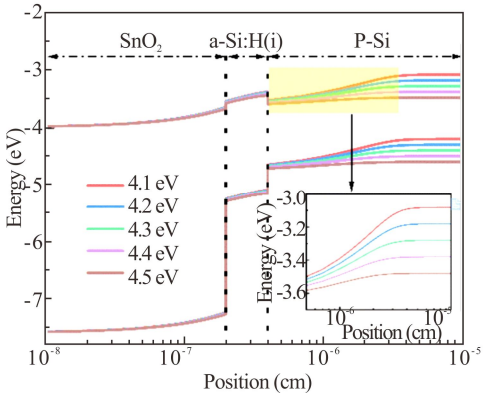

Fig.9 Band diagrams of SnO_2 with different *WFs*

If the experimental cell structure was pyramid shaped, it could not be completely covered by a 1-nm-thick a-Si:H (i) layer, and current leakages will likely occur. In the experimental design, we thus chose a 3-nm-thick a-Si:H (i) passivation layer. After optimizing each layer, we obtained a DASH solar cell with the V_{oc} of 693.1 mV, the J_{sc} of 43.34 mA/cm^2, the *FF* of 70.17%, and the η of 21.08%. The current-voltage (*I-V*) characteristic of the optimized cell is plotted in Fig.12.

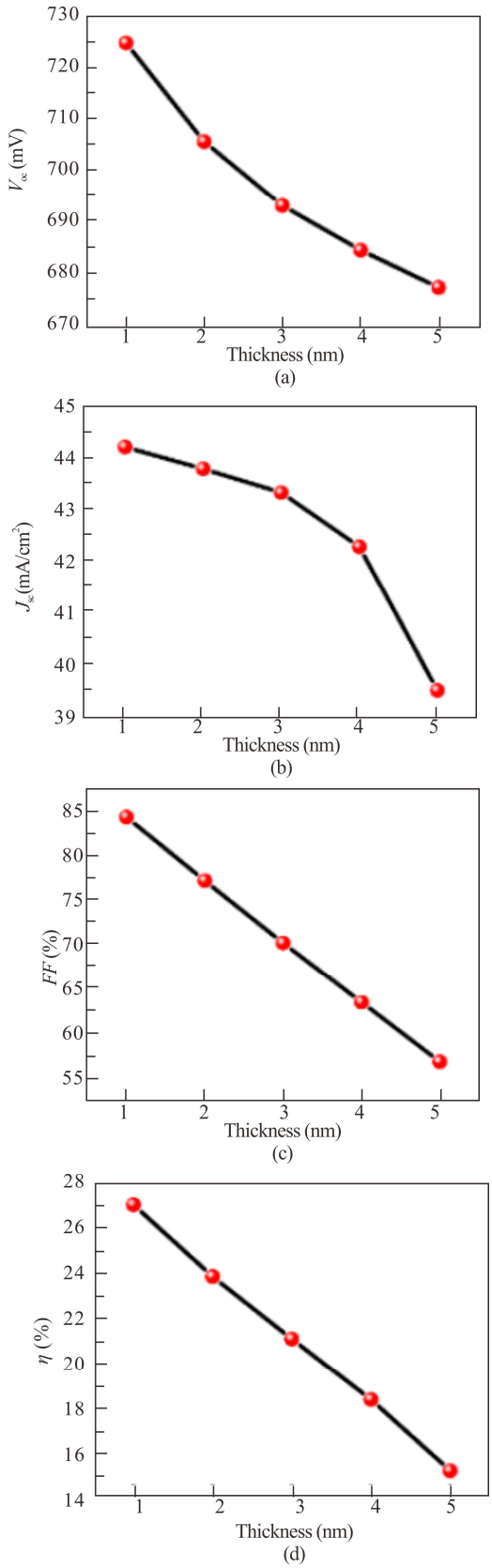

Fig.10 Performance parameters versus a-Si:H (i) thickness in DASH solar cells: (a) V_{oc}; (b) J_{sc}; (c) *FF*; (d) η

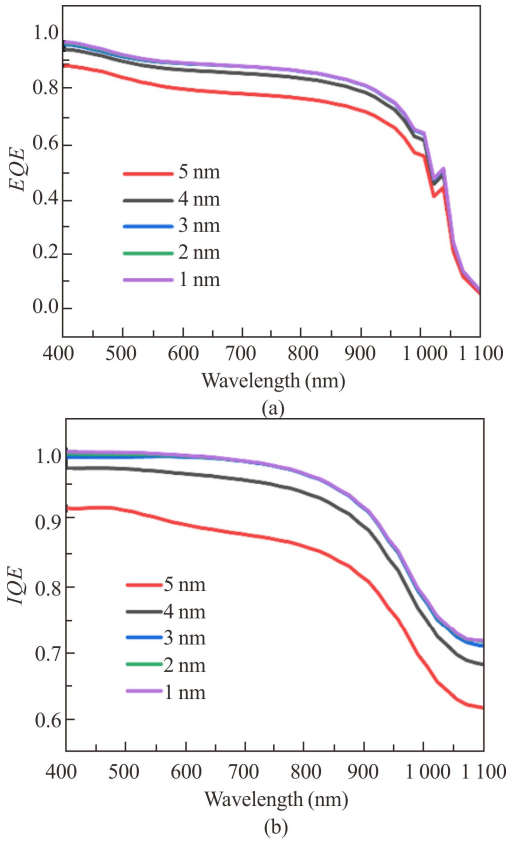

Fig.11 Spectra of (a) *EQE* and (b) *IQE* in DASH solar cells with different a-Si:H (i) thicknesses

Finally, we simulated the performance and stability of the optimized device in the temperature range of 260—340 K. As shown in Fig.13(a), V_{oc} decreases with increasing temperature, which may be due to the excitation thermal vibrations of electrons and holes that increase the complexation rate of electron-hole pairs upon temperature rise, and combined with the analysis of the efficiency plot in Fig.13(d), the device performs poorly at high temperatures of 360 K. For most semiconductors, the band gap decreases with increasing temperature. Therefore, the solar cell responds to the longer wavelength region of the solar spectrum, so the short-circuit current density increases with increasing temperature. From Fig.13(c), we can see that the *FF* of the device decreases sharply at 260 K, thus indicating that the *FF* greatly limits the efficiency of the device at low temperatures. Finally, we find that the optimal temperature suitable for the device structure is 290 K, when V_{oc} is 716.1 mV, J_{sc} is 43.3 mA/cm^2, *FF* is 70.01%, and efficiency is 21.71%.

To optimize the structure of undoped asymmetric solar cells, we simulated an Al/SnO_2/a-Si:H (i)/c-Si (p)/a-Si:H (i)/NiO_x/Ag structure using AFORS-HET software and optimized the band gap energy, electron affinity, thickness, and *WF* of the hole transport layer. The thickness and *WF* of the electron transport layer were also optimized, and the thickness of the a-Si:H (i) passivation

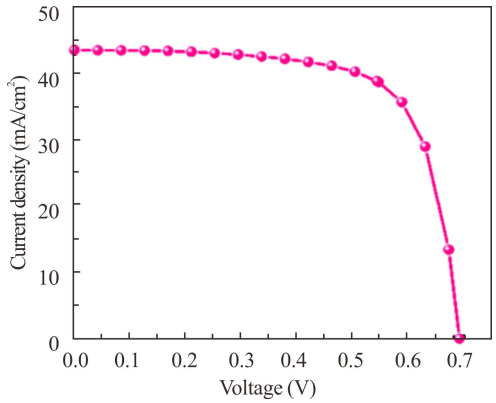

Fig.12 *I-V* characteristic of the optimized DASH solar cell (V_{oc}=693.1 mV, J_{SC}=43.34 mA/cm^2, *FF*=70.17%, η=21.08%)

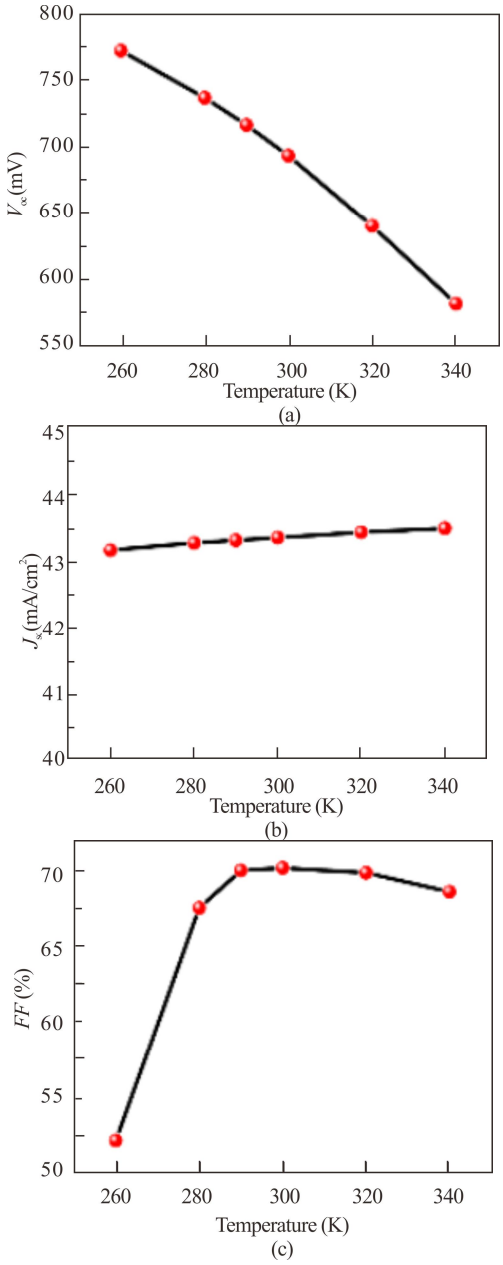

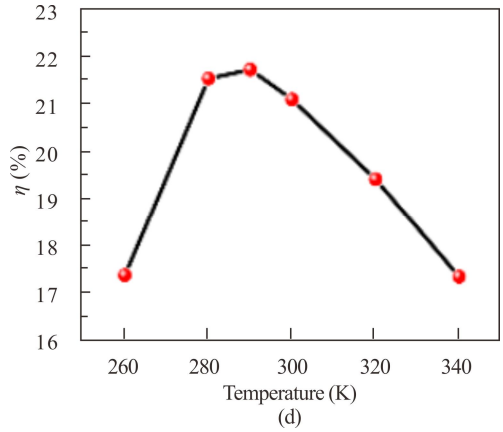

Fig.13 Performance parameters versus temperature in DASH solar cells: (a) V_{oc}; (b) J_{sc}; (c) *FF*; (d) η

layer was adjusted to improve the efficiency of the DASH solar cell. After optimization, this solar cell at 300 K has the V_{oc} of 693.1 mV, the J_{sc} of 43.34 mA/cm^2, the *FF* of 70.17%, and the η of 21.08%.

Ethics declarations

Conflicts of interest

The authors declare no conflict of interest.

References

[1] BULLOCK J, HETTICK M, GEISSBÜHLER J, et al. Efficient silicon solar cells with dopant-free asymmetric heterocontacts[J]. Nature energy, 2016, 1(3): 1-7.

[2] BATTAGLIA C, YIN X, ZHENG M, et al. Hole selective MoO_x contact for silicon solar cells[J]. Nano letters, 2014, 14(2): 967-971.

[3] BULLOCK J, WAN Y, XU Z, et al. Stable dopant-free asymmetric heterocontact silicon solar cells with efficiencies above 20%[J]. ACS energy letters, 2018, 3(3): 508-513.

[4] ZHONG S, DREON J, JEANGROS Q, et al. Mitigating plasmonic absorption losses at rear electrodes in high-efficiency silicon solar cells using dopant-free contact stacks[J]. Advanced functional materials, 2020, 30(5): 1907840.

[5] HOSSAIN M I, HASAN A K M, QARONY W, et al. Electrical and optical properties of nickel-oxide films for efficient perovskite solar cells[J]. Small methods, 2020, 4(9): 2000454.

[6] NAPARI M, HUQ T N, HOYE R L Z, et al. Nickel oxide thin films grown by chemical deposition techniques: potential and challenges in next-generation rigid and flexible device applications[J]. InfoMat, 2020, 3(5): 536-576.

[7] GONG Y, ZHANG S, GAO H, et al. Recent advances and comprehensive insights on nickel oxide in emerging optoelectronic devices[J]. Sustainable energy & fuels, 2020, 4(9): 4415-4458.

[8] SEGALINA A, LEBEGUE S, ROCCA D, et al. Structure and energetics of dye-sensitized NiO interfaces in water from Ab initio MD and large-scale GW calculations[J]. Journal of chemical theory and computation, 2021, 17(8): 5225-5238.

[9] SAJID S, ELSEMAN A M, HUANG H, et al. Breakthroughs in NiO_x-HTMs towards stable, low-cost and efficient perovskite solar cells[J]. Nano energy, 2018, 51: 408-424.

[10] PANT N, YANAGIDA M, SHIRAI Y, et al. Effect of different surface treatments of sputtered NiO_x on the photovoltaic parameters of perovskite solar cells: a correlation study[J]. Applied physics express, 2020, 13(2): 025505.

[11] LEE Y H, SONG H E, KIM K H, et al. Investigation of surface reactions in metal oxide on Si for efficient heterojunction Si solar cells[J]. APL materials, 2019, 7(7): 071106.

[12] WANG Z, LEE S H, KIM D H, et al. Effect of NiO_x thin layer fabricated by oxygen-plasma treatment on polymer photovoltaic cell[J]. Solar energy materials and solar cells, 2010, 94(10): 1591-1596.

[13] SUN H, CHEN S C, HSU S W, et al. Microstructures and optoelectronic properties of nickel oxide films deposited by reactive magnetron sputtering at various working pressures of pure oxygen environment[J]. Ceramics international, 2017, 43: S369-S375.

[14] JIANG Q, ZHANG X, YOU J. SnO_2: a wonderful electron transport layer for perovskite solar cells[J]. Small, 2018, 14(31): 1801154.

[15] XIONG L, GUO Y, WEN J, et al. Review on the application of SnO_2 in perovskite solar cells[J]. Advanced functional materials, 2018, 28(35): 1802757.

[16] DALAPATI G K, SHARMA H, GUCHHAIT A, et al. Tin oxide for optoelectronic, photovoltaic and energy storage devices: a review[J]. Journal of materials chemistry A, 2021, 9(31): 16621-16684.

[17] WANG D, LIU S, SHAO M, et al. Design of SnO(2) aggregate/nanosheet composite structures based on function-matching strategy for enhanced dye-sensitized solar cell performance[J]. Materials (Basel), 2018, 11(9): 1774.

[18] OPPONG-ANTWI L, HUANG S, LI Q, et al. Influence of defect states and fixed charges located at the a-Si: H/c-Si interface on the performance of HIT solar cells[J]. Solar energy, 2017, 141: 222-227.

[19] AHMMED S, AKTAR A, RAHMAN M F, et al. A numerical simulation of high efficiency CdS/CdTe based-solar cell using NiO HTL and ZnO TCO[J]. Optik, 2020, 223: 165625.

[20] ZHONG S, HUA X, SHEN W. Simulation of high-efficiency crystalline silicon solar cells with homo-hetero junctions[J]. IEEE transactions on electron devices, 2013, 60(7): 2104-2110.

[21] BORAH C K, TYAGI P K, KUMAR S. The prospective application of a graphene/MoS_2 heterostructure in Si-HIT solar cells for higher efficiency[J]. Nanoscale advances, 2020, 2(8): 3231-3243.

[22] STEIRER K X, NDIONE P F, WIDJONARKO N E, et al. Enhanced efficiency in plastic solar cells via energy matched solution processed NiO_x interlayers[J]. Advanced energy materials, 2011, 1(5): 813-820.